# Chapter 6

# Exploring the Galaxy–Absorption Connection

If galactic fountains, chimneys, supershells, cannonballs, or other mechanisms which invoke correlated supernovae explosions to power the outbreak of gas from galactic disks contribute to the replenishment of halo gas, then the QSO absorption line strengths should be correlated to signs of recent star formation. In the chimney model, the gas circulation time is $(3 - 5) \times 10^7$ yrs (Norman & Ikeuchi 1989). The picture is that $\approx 1$ kpc superbubbles can be formed if sequential supernovae explosions occur every $10^5$ yrs during the $10^7$ yr lifetime of a giant molecular cloud (Tomisaka, Habe, and Ikeuchi 1981). The cooling time of the gas is $\approx 10^6$ yrs at densities of $10^{-2}$ cm$^{-3}$. From these sequential supernovae explosions, chimneys can form with cool dense walls of neutral gas and central outward flows of hot gas ($T \approx 3 \times 10^7$ at the chimney base), which cool due to adiabatic losses and then finally by radiative losses as it rises to the top of the halo. The chimneys trace the spiral arms, and will be on the order of thousands in number for a given galaxy. The OB star formation regions (knots in spiral arms) should be detectable in intermediate $z$ HST images. Perhaps there is a correlation between the number of OB associations and the strength of absorption or the detailed kinematic structure inferred from the QSO absorption lines. Additionally, color indices for known morphological types can be used to look for evidence suggestive of star formation in these galaxies, which can then be compared to the absorption line strengths.

Presently, no significant trend of equivalent width with star formation rate has been found; that is not to say there is no connection, but the numbers are much too small statistically (since small impact parameters and large equivalent widths are actually quite rare) to make any trend show up as significant. One thing that is known, is that massive galaxies with high star formation rates are very rare, and the bluest galaxies (highest "specific" star formation rates) tend to be the smallest, as determined from the K–band light. So most of the blue absorbers cannot be Sb's (the average Mg II absorber color) with high star formation rates. It is possible that with detailed information on individual systems something might come out of all this, but nothing statistical has emerged at the present time because of the presently small numbers. (Steidel, private communication)

## 6.1 Executive Summary

We present HIRES/Keck spectra having resolution $\sim 6$ km s$^{-1}$ of Mg II $\lambda 2796$ absorption profiles which arise in the gas believed to be associated with 15 identified galaxies over the redshift range ($0.5 \leq z \leq 0.9$). These galaxies have measured redshifts consistent with those seen in absorption. Using non–parametric rank correlation tests, we searched for correlations of the absorption strengths, saturation, and line–of–sight kinematics with the galaxy redshifts, rest frame $B$ and $K$ luminosities, rest $\langle B-K \rangle$ colors, and impact parameters $D$. We found no correlations at the $2.5\sigma$ level between the measured absorption properties and galaxy properties. Of primary significance is the fact that the QSO–galaxy impact parameter apparently does not provide the primary distinguishing factor by which absorption properties can be characterized. The absorption properties of Mg II selected galaxies exhibit a large scatter, which, we argue, is suggestive of a picture in which the gas in galaxies arises from a variety of on–going dynamical events. Inferences from our study include: (1) The spatial distribution of absorbing gas in and around galaxies does not appear to follow a simple galactocentric functional dependence, since the gas distribution is probably highly structured. (2) A *single* systematic kinematic model apparently cannot describe the observed velocity spreads in the absorbing gas. It is more likely that galaxy/halo events giving rise to absorbing gas each exhibit their own systematic kinematics, so that a heterogeneous population of sub–galaxy scale structures are giving rise to the observed cloud velocities. (3) The absorbing gas spatial distribution and overall kinematics may depend upon gas producing events and mechanisms that are recent to the epoch at which the absorption is observed. In any given galaxy, these distributions likely change over a $\sim$ few Gyr timescale (few dynamical times of the absorbing clouds), which provides one source for the observed scatter in the absorption properties. Based upon these inferences, we note that any evolution in the absorption gas properties over the wider redshift range ($0.4 \leq z \leq 2.2$) should be directly quantifiable from a larger dataset of high–resolution absorption profiles.

## 6.2 Introduction

The Mg II doublet, as seen in absorption in the spectra of background QSOs (cf. Steidel & Sargent 1992), is known to arise in the low ionization gas associated with a population of "normal" field galaxies that exhibit little to no evolution in their rest frame $\langle B-K \rangle$ colors since a redshift of $z \sim 1.0$ (Steidel, Dickinson, & Persson 1994, hereafter SDP). Galaxies selected by the known presence of Mg II absorption represent a wide range of colors, from late–type spirals to the reddest ellipticals, have $L_B$ and $L_K$ luminosity functions consistent with local luminosity functions in which morphological types later then Sd are excluded, and exhibit a strong correlation between color and $L_K$ (fainter galaxies are bluer). These facts suggests that a wide range of morphological types are undergoing the processes that give rise to Mg II absorbing gas, but that isolated low mass ($L_K < 0.07L_K^*$) "faint blue galaxies" are not.

Now that we have a first look at what types of galaxies are being selected by their Mg II absorption cross section, we can undertake studies from which we hope to infer the spatial distribution and line–of–sight kinematics of the absorbing gas and to examine connections, if any, between the absorbing gas and galaxy properties. If correlations between galaxy and absorption properties can be established, where galaxies are directly accessible to imaging and spectroscopy, then we may be able to infer the properties of higher redshift galaxies simply by classifying their absorption properties. The hope is that we may chart the general evolution of galaxies and of their gas kinematic, chemical, and ionization conditions back to the epoch of the earliest QSOs (Steidel 1993; Bergeron et al. 1994; Welty et al. 1996; Charlton & Churchill 1996a; Bechtold 1996; Churchill & Vogt 1996).

A more direct motive for this study is to examine the model of $z \leq 1$ galaxy halos suggested by Lanzetta & Bowen (1990, 1992). They suggested that intermediate redshift galactic halos are roughly identical, have absorbing gas spatial number density distributions $\propto r_{\rm gal}^{1-2}$, and likely exhibit systematic rotational or radial flow kinematics. The primary test for this picture is the prediction that the *observed* differences in the absorption properties from one system to another are predominantly due to the QSO–galaxy impact parameter.

Based upon several studies (Petitjean & Bergeron 1990; Bergeron & Boissé 1991; Lanzetta 1992; Le Brun et al. 1993; Steidel 1993b; Bowen, Blades, & Pettini 1995; Steidel 1995), a consensus has emerged in which the "galaxy/halo" model (first proposed by Bahcall & Spitzer 1969) is favored over the "galactic fragments" (cf. Yanny 1992) and "dwarf satellites" (York et al. 1986) models. Whatever the true nature of Mg II absorbing gas, the bottom line is that a relatively luminous galaxy within $\sim 40$ kpc of the QSO line of sight appears to be a prerequisite for the detection of Mg II absorption (Steidel 1995). If all scenarios contribute at some level, statistical correlations between absorption and galaxy properties predicted by the galaxy/halo model (Lanzetta & Bowen 1992; Lanzetta 1992; Charlton & Churchill 1996b) would be "diluted" by the more stochastic kinematics expected from merging dwarf satellite galaxies or accreting *gaseous* sub–galactic fragments. That is, if the local environments around Mg II absorbing galaxies are populated by satellite galaxies and by fragments of on–going galaxy/halo events (i.e. accretion, superbubbles, merging), systematic trends with impact parameter, or any other galaxy property, would be difficult to detect due to a large scatter in the absorption properties.

In this paper, we report on observations of the Mg II $\lambda 2796$ absorption line obtained with a resolution of $\sim 6$ km s$^{-1}$ and signal–to–noise ratios $\sim 30$, and explore correlations between the absorption properties and the IR/optical luminosities and colors, impact parameters, and redshifts of the identified associated galaxies.

## 6.3 Observations

We observed the 11 QSOs presented in Table 6.1 with the HIRES echelle spectrometer (Vogt et al. 1994) on the Keck 10–m telescope on 1995 January 23–25. The spectral resolution was 6.6 km s$^{-1}$ ($R = 45,000$). There are small gaps in the spectra redward of 5100 Å where the free spectral range of the echelle format exceeds the width of the $2048 \times 2048$ Tektronix CCD. The spectroscopic sample was taken from the absorption line survey of Steidel & Sargent (1992) and was selected on the basis that each absorption system was associated with an imaged galaxy that had been spectroscopically confirmed to have the same redshift as seen in absorption (SDP).

The galaxy properties were obtained from broad–band $g(4900/700)$, $\Re(6930/1500)$, $i(8000/1450)$ and NICMOS images of the QSO fields. This combination of filters allowed the rest–frame $B$ and $K$ magnitudes of the galaxies to be determined. A brief description of the imaging and follow–up spectroscopic work has been presented by SDP and Steidel & Dickinson (1995). Here, we concentrate on the properties of the 15 identified $z \leq 1$ absorbing galaxies for which we have acquired HIRES QSO absorption line spectra.

## 6.4 Analysis

The HIRES data were reduced with the IRAF[1] Apextract package for echelle data. We have identified absorption features in the spectra using the method presented by Lanzetta, Turnshek, & Wolfe (1987), where we have chosen a bandpass of 2.3 resolution elements (i.e. 7 pixels). A detection level of $5\sigma$ was enforced and features having Mg II rest equivalent widths $W_{\rm min} < 0.01$ Å were discarded. This latter criterion enforced a uniform detection level upon all absorption systems at the level of the lowest signal–to–noise ratio spectrum in the sample.

Voigt profiles (natural + thermal broadening) convolved with the instrumental broadening (Gaussian with $\sigma = 2.46$ km s$^{-1}$) were fit to the profile substructures using an interactive profile–fitting algorithm of our own design. In all cases, the Mg II doublet and at least one unsaturated weaker transition from either Fe II or Mg I were fit simultaneously. Thus, in the cases where the Mg II profiles appear saturated, there was little ambiguity in both the number of subcomponents and their relative velocities. In Figure 6.1, we present the profile fits to the QSO absorption lines observed from G2, which is the $z = 0.8514$ galaxy in the Q0002+051 field. Of the 15 systems used for this study, these profiles are the most complex. As such, this system serves as an illustration of the level of information available for our profile fits and the "accuracy" of the these fits over a range of subcomponent structures.

In Figure 6.2, we present the HIRES Mg II $\lambda 2796$ absorption profiles in units of rest frame line–of–sight velocity. The velocity spread of each panel is 400 km s$^{-1}$, except for G2, which is 800 km s$^{-1}$. For illustration purposes (to allow a comparison of absorption strengths and subcomponent variations with the projected galactocentric distance probed by the line of sight), we have sequenced the profiles in order of increasing QSO–galaxy impact parameter, $Dh^{-1}$ kpc[2].

To quantitatively ascertain if any connections between the low ionization gas absorption strengths and line–of–sight kinematics and the galaxy properties are present in our sample, we characterized the profiles by the number of subcomponents, $N_{\rm c}$, or "clouds", and three simple kinematic indicators. Since we assume no *a priori* knowledge of the gas kinematics, we have developed crude empirical indicators that are model independent. The first kinematic indicator is the "absolute deviation from the median" of the cloud

[1]IRAF is distributed by the National Optical Astronomy Observatories, which are operated by AURA, Inc., under contract to the NSF.

[2]We assume $q_0 = 0.05$ and quote all distances in terms of $h = H_0/100$ km s$^{-1}$ Mpc$^{-1}$.

velocities,

$$A(\Delta v) = \frac{1}{N_{\rm c}} \sum_{i=1}^{N_{\rm c}} |\Delta v_i| \,, \qquad (6.1)$$

where $\Delta v_i = v_i - \bar{v}$, and $\bar{v}$ is the median cloud velocity.

The median is used in lieu of the average because the former is symmetric about the number of clouds and is not sensitive to one or a few large $\Delta v_i$ clouds. The second kinematic indicator is the number of absolute deviations of the highest velocity cloud,

$$N_A = \frac{\max(\Delta v^{+}, |\Delta v^{-}|)}{A(\Delta v)}, \qquad (6.2)$$

where $\Delta v^{+}$ and $\Delta v^{-}$ are the largest redshifted and blueshifted cloud velocity differences from the system median, respectively. This quantity, which ranges between $1 \leq N_A \leq 4$ for our data, measures the degree and presence of an extreme kinematic "outlier" in each system. The third kinematic indicator is a measure of the kinematic asymmetry,

$$\eta = \frac{\min(\Delta v^{+}, |\Delta v^{-}|)}{\max(\Delta v^{+}, |\Delta v^{-}|)}, \qquad (6.3)$$

where $\eta = 1$ indicates that the extreme redshifted and blueshifted clouds lie symmetrically about the system median, and small $\eta$ indicates high asymmetry.

## 6.5 Testing For Correlations

We ran non–parametric Spearman and Kendall correlation tests on the measured galaxy and absorption properties, which are presented in Table 6.2. The Kendall tests better handle the treatment of data in which a value appears multiple times (fractional ranks), as is the case with $N_{\rm c}$. Galaxies for which a given property was not measured were excluded from the test pertaining to the missing property. Using the criterion $P_{\rm k} \leq 0.01$ (99% probability that no correlation is not consistent with the data) to indicate the presence of a correlation, we found *no* statistically significant correlations between the absorbing gas strengths or kinematics with the galaxy properties. To examine the effects due to projected galactocentric distance, $D$, and due to path length through the halo, $S = 2\sqrt{R^2 - D^2}$, where $R = 38h^{-1}(L_K/L_K^{*})^{0.15}$ (Steidel 1995), we ran additional tests on the absorption properties versus $D/R$ and $S$, and versus $L_B$ and $L_K$ normalized by $D$ and by $S$. One might expect correlations to be revealed from the normalized $L_K$ if absorbing gas exhibited a smooth radial spatial distribution that scales with the luminosity to some power, as expected for pressure–confined clouds in halos where the pressure gradient scales with galaxy mass (Mo & Miralda–Escudé 1996). Again, we found no correlations.

To investigate sensitivity to small–number statistics, and to ascertain if our sample of 15 galaxies is a fair representation of the SDP sample, we also performed Monte–Carlo rank correlation tests. For each simulation, we assigned the observed absorption properties (columns 8–13 in Table 6.2) to 15 galaxies drawn at random from 54 $z \leq 1$ SDP galaxies. For each correlation test, 5000 of these simulations were executed and the probability $P_{\rm MC}$ that the measured $\tau_k$ or greater would be measured from randomized galaxy–absorption properties for our sample was computed. The $P_{\rm MC}$ strongly correlate with the $P_{\rm k}$, which is indicative that our sample is a representative subset of the SDP data set and that the measured $P_{\rm k}$ are reliable indicators.

In Table 6.3, we present those tests for which both the simulated and measured $P$ are weakly suggestive of correlations in that the null hypothesis (no correlation) is not consistent with the data at the $2\sigma$ confidence level ($P_{\rm k} \leq 0.1$). Since one or a few kinematically simple or complex systems could be dominating a test for which a correlation is suggested at the $\sim 2\sigma$ level, we re–ran the Spearman and Kendall tests on our sample, each time omitting a single galaxy. We then examined the *distribution* of $P_{\rm k}$ for each test to see if a large $P_{\rm k}$ results from the omission of any one galaxy. For the correlation tests tabulated in Table 6.3, the $P_{\rm k}$ distributions cluster tightly about the their respective values, except for $A(\Delta v)$ versus $S$ (note the discrepancy between $P_{\rm k}$ and $P_{\rm MC}$ for this case).

## 6.6 A Second Look at the Galaxy/Halo Model

We further investigated the "halo" model described by Lanzetta & Bowen (1990, 1992). As stated above, the primary test of this model is the prediction that the observed differences in the absorption properties from one system to another are predominantly due to the QSO–galaxy impact parameter. Thus, we performed maximum likelihood least squares linear fits (LSFs) to the quantities tested against impact parameter that are listed in Table 6.3. The goal is to obtain the significance level of each fitted slope. If any of these LSF slopes is not inconsistent with zero, within the uncertainties applied to the data, then we may have further evidence supportive of a possible correlation.

For the LSF fits, we modeled the uncertainty of each absorption property as scatter due to Poisson fluctuations, which are predicted from the fact that the QSO line of sight samples a finite number of clouds in each galactic system. For the equivalent widths [cf. Equation 2 of Lanzetta & Bowen (1990)], the LSF uncertainty is given by,

$$\sigma = \left\{ \sigma^2(W_{\rm r}) + k^2[W_{\rm r}/k + 1] \right\}^{1/2}, \tag{6.4}$$

where $\sigma(W_{\rm r})$ is the measured uncertainty in $W_{\rm r}$ and the "scatter" term follows from Poisson counting statistics if the $W_{\rm r}$ are correlated with $N_{\rm c}$, following $W_{\rm r} = kN_{\rm c}$ (Petitjean & Bergeron 1990). We obtained the LSF relation $k = 0.0703 \pm 0.0002$ to the data presented in Figure 6.3. The value of $k$ may actually depend upon redshift, but can be approximated as a constant over $0.5 \leq z \leq 0.9$, since $W_{\rm r}$ and $N_{\rm c}$ for our sample do not correlate with $z$. If unresolved sub–components remain hidden in the HIRES profiles, our measured $k$ would be an upper limit. A smaller $k$ would result in smaller modeled scatter.

In Figure 6.4, we plot the total absorption strength, $W_{\rm r}$, verse impact parameter, D$h^{-1}$ kpc. The solid circles are taken from Table 6.2, where the error bars are the modeled scatter as described above. The open circles are the full $z \leq 1$ SDP data set, which we presented to illustrate that our subsample appears to be a fair representation of the full available sample. Applying the modeled scatter as uncertainties in $W_{\rm r}$, we found that an LSF to the relation $W_{\rm r} = aD^{\alpha}$ yields $\alpha = -0.28 \pm 0.50$ with $\chi^2_\nu = 1.3$. Thus, we found no anti–correlation at the 99.9% confidence level of $W_r$ with $D$ for our 15 systems. Apparently, the spatial number density of "halo" absorbing clouds does not follow a simple power law with galactocentric radius. For comparison, we also show the LSF fit obtained by Lanzetta & Bowen (1990) to a similar size but different data set (not shown). Our LSF fits to $\mathrm{DR} = \alpha D + A$ and $N_c = AD^{\alpha}$ both yielded slopes statistically consistent with $\alpha = 0$, where we have assigned statistical scatter (uncertainties) to DR and $N_c$ consistent with those of the $W_r$.

It is important to consider whether non–unique solutions for the profile fits, as illustrated in Figure 6.1, could significantly effect our conclusions. Consider the number of clouds, $N_c$, which is a very central quantity in that it either directly or indirectly effects the computed values of the kinematic indicators. Our fitting philosophy was to introduce the *minimum* number of subcomponents that yielded model spectra consistent with the constraints provided by the error spectra. Thus, the $N_c$ are lower limits, since finite signal–to–noise and instrumental resolution could conceal narrow subcomponents. The modeled Poisson fluctuations in the $N_c$ are typically a factor of a few larger than the uncertainty from the profile fits, though this is difficult to precisely quantify. Our results would be altered only if there was some unknown systematic error in the fitted $N_c$ with the impact parameter, $D$, *and* if the uncertainty in the fitted $N_c$ were roughly the same size as the modeled scatter.

That we have found no dependence of $N_c$ with $D$ has implications for predictions from systematic rotational and radial flow kinematic models. In particular, consider the median absolute deviation, $A(\Delta v)$, versus QSO–galaxy impact parameter, which we have plotted in Figure 6.5. Since the number of clouds is independent of $D$, we can approximate $A(\Delta v) \propto \langle \Delta v \rangle$, the mean $\Delta v_i$. For infall models, $\langle \Delta v \rangle \propto (1 - D^2/R^2)^{1/2}$, and for rotational models, $\langle \Delta v \rangle \propto 1 - D/R$, where $R$ is the "halo" or "disk" size. Both models predict that $A(\Delta v)$ decreases with $D$ and sharply cuts off at $D = R$. There is no such anti–correlation in our sample. In fact, the Spearman and Kendall tests are weakly suggestive of a correlation, not the predicted anti–correlation. For the case of rotation in disk galaxies, it is likely that for $D \leq 20$ kpc, the random inclination of disk galaxies would introduce a sizable scatter in the $A(\Delta v)$. We note, however, that this scatter would always be toward smaller $A(\Delta v)$ values as disk inclination decreases, and thus there would still be an $A(\Delta v)$ versus $D$ upper envelope that does exhibit an anti–correlation.

Overall, what is clear, is that the absorption properties of Mg II absorption–selected galaxies exhibit a level of scatter greater than that predicted by simply assuming Poisson fluctuations on the grounds that each line of sight is sampling a finite number of clouds. Based upon 15 systems, we cannot conclude (with confidence) that weak correlations do or do not exist between the quantified kinematic properties of the absorbing gas and the galaxy properties available from ground–based images, but we can argue, based upon the above discussion, that "smooth" correlations can be ruled out. *Of primary significance is the fact that the QSO–galaxy impact parameter apparently does not provide the primary distinguishing factor by which absorption properties can be characterized.*

The implications are that (1) the spatial distribution of absorbing gas surrounding intermediate redshift galaxies is not smoothly varying, and that (2) the velocities of the absorbing gas clouds cannot be described by a *single* systematic kinematic model. One may infer that these quantities may not be roughly identical from galaxy to galaxy of similar morphological type, even if the events and processes that give rise to the gas are. Such a picture is difficult to reconcile with theoretical results that predict a "steady state" in which cloud coalescence and growth from the cooling of hot gas in a virialized halo is balanced by cloud disruption and evaporation, giving rise to a near unity covering factor (cf. Mo & Miralda–Escudé 1996; Anninos & Norman 1995; Begelmann & McKee 1990). A "steady state" halo of this type would likely show systematic trends with less scatter than is observed, and is not well supported by observations of local galaxies (Bowen, Blades, & Pettini 1995), provided there is no rapid halo evolution from $z \sim 0.4$ to the present.

## 6.7 Discussion

If Mg II absorption profiles contain spectroscopic imprints of systematic spatial and velocity distributions of the low ionization gas comprising disks and halos, as suggested by Lanzetta & Bowen (1992), it appears from our results that absorbing gas would have to arise from a heterogeneous population of events and mechanisms that each impart their own systematic kinematic signatures, and possibly chemical and ionization conditions. From lines of sight through the Milky Way, the Large Magellanic Cloud (LMC), and local galaxies, a substantial variation in the absorption properties corresponding to a variety of dynamical events has been observed (Savage et al. 1993; Lu, Savage, & Sembach 1994; Cardelli, Sembach, & Savage 1995; Sembach, Savage, & Lu 1995; Bowen, Blades, & Pettini 1995; Caulet & Newell 1996). In the vicinity of a "typical" Mg II absorption–selected galaxy, such events would need to be on–going over a Hubble time in order to explain the sustenance of extended gaseous regions [as inferred from their non–evolving co–moving cross section (Steidel & Sargent 1992)], since the absorbing cloud lifetimes are $\sim 1$ Gyr (Lanzetta & Bowen 1990; Mo & Miralda–Escudé 1996).

Hubble Space Telescope (HST) WFPC2 images of $z \sim 1$ galaxies from the DEEP Project reveal a diversity of morphological types, including small compact galaxies, and apparently normal late–type spirals (Koo et al. 1996). These images also reveal evidence suggestive of a higher frequency of merging in the past and for interactions of small, gas–rich galaxies with each other or with larger, well–formed galaxies. Apparently, a mixture of physical processes is at work in the formation and evolution of field galaxies. Based upon local studies, Bowen, Blades, and Pettini (1995) have suggested that recent merging events may play an important role in the presence of Mg II absorbing gas, and caution against a generalized halo model.

On the other hand, one cannot completely rule out the idea that some fraction of the observed systems are dwarfs (i.e. similar to Carina, Leo I, etc.) that undergo episodic self–regulating star formation, resulting in the blow out of gas to large radii over a Hubble time. Occasionally, a gas rich low mass galaxy could lie within $D \sim 50$ kpc and $\Delta v \sim 100$ km s$^{-1}$ of an "identified" galaxy by virtue of projection, especially in the instances when "double galaxies", which are suggestive of Local Group environments, are seen to be associated with Mg II and/or C IV absorption. However, it is difficult to reconcile a large contribution from this latter picture due to an observed correlation of the absorption cross–section with the identified galaxy $K$ luminosity (Steidel 1995). This correlation suggests that galactic mass has some connection with a galaxy's ability to organize tidally stripped, accreting, or infalling material (cf. Mo & Miralda–Escudé 1996; Steidel 1995). The important point here is that unbiased deep imaging and thorough spectroscopic surveys of QSO fields are still in progress, and as shown by Charlton & Churchill (1996b), the simple picture of a near–unity covering factor "galactic halo" is not yet conclusively demonstrated.

Even though models of the spatial distributions and kinematics of the Mg II absorbing gas around galaxies are still not well constrained by the observations, there is little doubt that the galaxies identified with Mg II absorption are indeed associated in some way with the processes that give rise to the absorbing gas (SDP; Steidel 1995). As such, the types and frequencies of the *events* that give rise to absorbing gas are likely to show trends with galaxy morphologies and impact parameter, even if there is a great deal of scatter in these trends. It remains to be understood to what degree extended and warped H I disks in spiral galaxies contribute to absorption at all impact parameters (Charlton & Churchill 1996b), though it is highly probable that they actually dominate for $D \leq 20h^{-1}$ kpc and perhaps can even account for most strong saturated components out to $D \leq 40h^{-1}$ kpc. It is interesting to note the extended and complex structure of high column density H I gas surrounding M81, which is seen to be distributed in a flattened geometry and is associated with *current* satellite mergings (Yun, Ho, & Lo 1994). This observation also supports the idea that for $r_{\rm gal} \geq 20$ kpc and for the range of observed morphological types, likely sources of gas are the tidal stripping of or blow out from orbiting dwarf satellite galaxies (Wang 1993), the presence of dwarf galaxies very close to the QSO line of sight (York et al. 1986), or the accretion of clumps (fragments) of intergalactic gas (Mo & Miralda–Escudé 1996). Since gas producing events (such as superbubbles) from both galaxies and dwarf companions give rise to similar absorption strengths and kinematics over a $\sim 50$ kpc galactocentric range of impact parameters [as seen for the Milky–Way and environs (Lu, Savage, & Sembach 1994; Caulet & Newell 1996; Welty et al. 1996)], it will be difficult to interpret the origins of absorbing gas until deep high–spatial resolution images of the galaxies can be incorporated into QSO absorption line studies.

Based upon the available data, one may tentatively infer that Mg II absorption–selected galaxies are roughly identical in the sense that they are continually processing and accreting gas, but differ in that the spatial and kinematic distribution of the gas *around* each galaxy depends upon the events recent to the epoch at which it is observed. It is likely that on–going gas processing events are continuously reorganizing sub–galaxy distributions of gas on timescales of a few Gyr. This is *not* to imply that global reorganization of gaseous kinematic, ionization, and spatial distributions occurs in all Mg II absorbing galaxies. We caution that the data do *not* rule out the idea that sub–galaxy distributions are somewhat stable but have a high level of structure, since it is possible that observations of a single galaxy and its surroundings along different lines of sight at a single epoch in its evolution could give rise to the wide variety of observed absorption profiles. A test of these issues would include establishing which, if any, of the following observed variations in absorption properties show some type of systematic trend: (1) galaxies of different morphological types, (2) similar lines of sight through galaxies of a given morphological type at different cosmic epochs, or (3) different lines of sight through galaxies of a given morphological type at a given cosmic epoch.

For example, statistical differences may exist between samples of profiles for the different morphological types. This might imply that the relative importance of the various on–going processes that produce and adjust the distribution of gas is different in the different morphological types. Similarly, there could be statistical differences between samples of profiles for galaxies of the same morphological types at different redshifts. This might be indicative that the relative importance of the various on–going processes is changing. Since ellipticals and spirals have distinctive internal stellar dynamics, their gas kinematics may also be distinctive, especially for $r_{\rm gal} \lesssim 20$ kpc. For both ellipticals and spirals, if the events at larger galactocentric radius arise predominately in satellite galaxies and/or are stochastic accretion events lasting $\sim$ few Gyr, they will be observable for the full range of observable $D$. Thus, the line–of–sight quantities $N_A$ and $\eta$ would be expected to exhibit scatter with $D$, since they may be sensitive to the chance interception of "active" halo material. As such, inferring the distinction between kinematic systematics based upon morphological type at small $D$ would be complicated. It will be an interesting exercise to try to separate out the absorption properties by galaxy morphology once the number of observed Mg II absorbing galaxies becomes large.

We are obtaining deep WFPC2 images of the QSO fields with the goal of obtaining further clues for interpreting the kinematics measured from HIRES profiles. In the case of spiral galaxies, inclination and orientation with respect to the line of sight may play an important role. It is interesting to compare G7, a face–on spiral, and G15, a highly inclined spiral, which have comparable $L_B$ luminosities, $N_c$, $N_A$, and $D$, but slightly different $K$ luminosities, and strikingly different absorption profile shapes. G7 exhibits lower column density clouds that are kinematically symmetric about the galaxy $z$ direction, whereas G15 exhibits higher column densities. The galaxy G2, which is a compact blue diskless galaxy, exhibits what appears to be a great deal of recent kinematic activity (see Figure 6.1) and a remarkably more complex absorption than is seen in the spirals G7 and G15. Perhaps the line of sight through G2 is sampling a recent and large accretion event.

## 6.8 Conclusions

As a first step toward developing a better appreciation of the spatial distributions and kinematics of low ionization absorbing gas associated with galaxies, we have presented the Mg II $\lambda 2796$ absorption profiles for 15 $z < 1$ galaxies, developed simple kinematic indicators of the profiles, and searched for statistically significant correlations between the absorbing gas and galaxy properties.

1. Using Spearman and Kendall non–parametric rank correlation tests, we found no evidence for $2.5\sigma$–level correlations between the absorbing gas and galaxy properties. We performed Monte–Carlo Spearman and Kendall tests in which we randomly assigned our measured absorption properties to the full SDP sample of galaxies. These tests revealed that our 15 galaxies are a fair representation of the SDP dataset and that the Spearman and Kendall results provide reliable indicators for the presence or non–presence of correlations.

2. In Table 6.3, we have listed the eight tests for which the Spearman and Kendall results are weakly suggestive of correlations. Since trends in absorption properties with the QSO–galaxy impact parameter, $D$, are an important test of the galaxy/halo model, we have performed maximum likelihood least square fits to those tests that included $D$ (i.e. DR, $N_c$, and $W_r$ versus $D$). For these fits, we modeled the uncertainty in the measured absorption properties as scatter due to Poisson fluctuations, which are predicted when sampling a finite number of absorbing clouds along the line of sight through a galaxy halo. All LSF slopes were consistent with zero, which is indicative of no statistically significant dependence with $D$ for these absorption properties.

3. Since the number of clouds shows no significant dependence with $D$, both the rotation and radial flow kinematic models predict an anti–correlation of the median absolute deviation of cloud velocities with impact parameter. As illustrated in Figure 6.5, we found no clear trend in $A(\Delta v)$ with $D$. If anything, the weak positive correlation suggested by the rank correlation tests is suggestive of a scenario in which more than one kinematic model may be needed to explain the data. Perhaps the inner 20 kpc are dominated by the systematic kinematics expected for galaxies (morphology dependent?), whereas the higher impact parameter kinematics is dominated by accretion and merging of various types of "halo" material.

4. We have found that the QSO–galaxy impact parameter apparently does not provide the primary distinguishing factor by which absorption properties can be characterized. This fact suggests that we should investigate the degree to which galaxy morphologies and, in the case of disk galaxies, orientations with respect to the QSO light path play a role in distinguishing between observed absorption properties.

5. Since Mg II absorption properties exhibit a level of scatter greater than that predicted by a simple Poisson fluctuation model, our data do not provide a level of constraint necessary for us to infer functional relations that describe the spatial and kinematic distributions of Mg II absorbing gas around galaxies. If weak correlations are in fact present, they exhibit a large enough scatter that a fair sample of 15 systems has not yielded unequivocal results.

6. As one possible interpretation, we have tentatively suggested a picture of intermediate redshift galactic halos in which the distribution and kinematics of the low ionization absorbing gas is dominated by the events and mechanisms that give rise to the gas recent to the epoch of observation. These halos would be dynamically active with evolving gaseous conditions dependent upon local environmental influences, as expected with tidally stripped dwarf satellite galaxies, infalling gaseous sub–galactic fragments, superbubbles, and in the case of disk galaxies, with high velocity clouds, galactic fountains, and the warped extended disks themselves. Our observational results are not suggestive of a picture in which galaxy halos underwent a single epoch of dynamical formation in the past. Rather, these galaxies have experienced multiple and episodic merging and have undergone internal events that give rise to extended (though somewhat patchy) regions of low ionization absorbing gas.

7. If the Mg II absorbing gas from these events has a dynamical time of $\sim 1$ Gyr, the gas producing events, spread out both spatially and temporally, would not give rise to halos comprised of multiple coalescing and evaporating absorbing clouds that yield a near–unity covering factor. Such halos would be expected to exhibit systematic kinematics and have an approximately spherically symmetric spatial number density distribution that scales with galactocentric radius. Instead, these events may give rise to $\sim$ few Gyr sub–galactic gaseous structures so that the overall spatial distribution and kinematics of absorbing gas in any one galaxy would be expected to change over a few cloud dynamical times. The important point is that the data are not suggestive of the continual processing of gas that would give rise to an apparently "steady state" halo over the 10 Gyr evolution of the galaxy.

8. Since the dynamical time is roughly an order of magnitude shorter than the overall look–back time over which complex Mg II absorption is seen around galaxies, and since QSO absorption lines likely sample gas produced in events recent to the epoch at which it is observed, we should be able to directly track evolution in the absorption properties. A larger database of HIRES Mg II profiles would be instrumental for directly quantifying evolution in the absorbing gas properties over the redshift range $0.4 \leq z \leq 2.2$. Such evolution may provide information helpful for ruling out various type of events or absorbing structures and for quantifying possible major shifts in epochs from one type of pre–dominant galaxy/halo gas processing phase to another.

A more comprehensive appreciation of the spatial and kinematic properties of low ionization absorbing will require a sizable unbiased sample of high resolution absorption profiles (unbiased in that the distribution of galaxy luminosities, colors, impact parameters, and absorption rest equivalent widths are consistent with having been drawn from the observed distributions of Mg II selected galaxies). It is important that surveys of QSO fields be complete to a small limiting rest frame luminosity and that the selection of these fields be unbiased with regard to the presence or non–presence of intervening absorbing galaxies.

Unless the gas kinematics in spiral/disk and elliptical galaxies are distinguishable as seen in high resolution profiles, it is not likely the Mg II absorption properties can be used to infer the type of galaxy associated with the absorbing gas at the highest redshifts, where the galaxy properties are difficult to obtain. However, we may be able to roughly infer the region of the galaxy sampled by the line of sight or something about its current or recent environmental dynamical activity. Ultimately, the observed evolutionary properties of gas derived from QSO absorption line studies are likely to yield direct quantities from which the formation and evolution time scales of $10^{12-13}$ $M_{\odot}$ structures in the universe can be better understood.

Table 6.1. The SDP QSOs

| QSO | V [mag] | $z_{\rm em}$ | Exp [s] | $W_{\rm min}(\lambda 2796)$ [Å] | |
|---|---|---|---|---|---|
| $0002+051$ | 16.2 | 1.899 | 2700 | 0.002 | 0.002 |
| $0117+212$ | 16.1 | 1.491 | 5400 | 0.004 | 0.004 |
| $0420-014$ | 17.0 | 0.915 | 3600 | 0.006 | |
| $0454+036$ | 16.5 | 1.343 | 4500 | 0.003 | |
| $1148+384$ | 17.0 | 1.299 | 5400 | 0.006 | |
| $1222+228$ | 15.5 | 2.040 | 3600 | 0.006 | |
| $1241+174$ | 15.4 | 1.282 | 2400 | 0.003 | |
| $1248+401$ | 16.3 | 1.032 | 4200 | 0.002 | |
| $1254+044$ | 16.0 | 1.018 | 2400 | 0.006 | 0.004 |
| $1317+274$ | 16.0 | 1.014 | 3600 | 0.004 | |
| $1622+235$ | 18.3 | 0.927 | 19240 | 0.010 | 0.009 |

Note. — The quoted exposure time is the sum of combined observations. The quantity $W_{\rm min}$ is the $5\sigma$ detection rest equivalent width limit of a feature in the velocity range $\pm 600$ km s$^{-1}$ from the absorber redshift. For the cases where two absorbers lie along the QSO line of sight, the second entry corresponds to the higher redshift system.

Table 6.2. Absorbing Galaxy Properties

| | | | Galaxy Properties | | | | Absorption Properties | | | | | |
|---|---|---|---|---|---|---|---|---|---|---|---|---|
| ID | QSO | $z_{\rm gal}$ | $L_B$ | $L_K$ | $B-K$ | $Dh^{-1}$ | $W_{\rm r}$ | DR | $N_{\rm c}$ | $A(\Delta v)$ | $N_A$ | $\eta$ |
| (1) | (2) | (3) | (4) | (5) | (6) | (7) | (8) | (9) | (10) | (11) | (12) | (13) |
| G1 | 0002 | 0.5914 | 1.09 | 1.34 | 4.12 | 23.8 | 0.11 | 1.51 | 1 | 5.2 | 1.06 | 0.89 |
| G2 | | 0.8514 | 1.23 | 0.47 | 2.86 | 18.5 | 1.14 | 1.11 | 14 | 105.7 | 3.60 | 0.17 |
| G3 | 0117 | 0.5763 | 2.32 | 2.54 | 4.00 | 5.1 | 0.91 | 1.07 | 4 | 31.2 | 2.10 | 0.77 |
| G4 | | 0.7289 | 3.27 | 3.65 | 4.02 | 36.0 | 0.24 | 1.67 | 5 | 49.9 | 1.00 | 0.90 |
| G5 | 0420 | 0.6330 | 0.28 | 0.34 | 4.11 | 10.3 | 0.86 | 1.32 | 9 | 59.9 | 3.24 | 0.32 |
| G6 | 0454 | 0.8596 | 0.26 | | | 10.6 | | | 12 | 45.5 | 1.68 | 0.91 |
| G7 | 1148 | 0.5532 | 0.75 | 0.56 | 3.59 | 13.4 | 0.60 | 1.61 | 8 | 47.7 | 1.95 | 0.79 |
| G8 | 1222 | 0.6681 | 0.49 | 0.45 | 3.80 | 26.9 | 0.48 | 1.51 | 6 | 79.5 | 2.80 | 0.18 |
| G9 | 1241 | 0.5507 | 0.64 | 0.41 | 3.42 | 13.8 | 0.50 | 1.37 | 4 | 39.6 | 3.48 | 0.25 |
| G10 | 1248 | 0.7725 | 0.53 | 0.27 | 3.15 | 23.2 | 0.69 | 1.25 | 8 | 53.6 | 3.87 | 0.23 |
| G11 | 1254 | 0.5192 | 0.14 | 0.11 | 3.65 | 16.2 | 0.55 | 1.49 | 6 | 70.6 | 3.61 | 0.14 |
| G12 | | 0.9341 | 0.43 | 0.26 | 3.35 | 8.3 | 0.36 | 1.51 | 2 | 20.5 | 1.56 | 0.77 |
| G13 | 1317 | 0.6598 | 2.30 | 2.10 | 3.80 | 37.7 | 0.34 | 1.55 | 8 | 61.0 | 1.55 | 0.66 |
| G14 | 1622 | 0.7967 | 1.63 | 0.74 | 3.04 | 46.5 | | | 4 | 55.1 | 1.36 | 0.77 |
| G15 | | 0.8915 | 0.71 | 0.33 | 3.07 | 15.0 | 1.53 | 1.12 | 6 | 47.7 | 1.79 | 0.95 |

Note. — Column 1 provides the galaxy ID number. Listed in column 2 are the first four digits which designate the QSOs listed in Table 1. The galaxy's redshift, and $B$ and $K$ luminosities (in terms of $L_B^*$ and $L_K^*$, respectively) are listed in columns 3, 4, and 5. The rest–frame $\langle B-K\rangle$ colors are listed in column 6, and the impact parameters in kpc are given in column 7. The absorption properties, measured from the HIRES spectra, include the rest–frame $\lambda2796$ equivalent width (column 8) and the doublet ratio DR $= W(\lambda2796)/W(\lambda2803)$ (column 9). Columns 10 and 11 list the number of clouds $N_{\rm c}$ and the mean absolute deviation of the clouds $A(\Delta v)$ in km s$^{-1}$. Column 12 lists the number of mean absolute deviations $N_A$ of the most extreme cloud and column 13 lists a measure of the velocity asymmetry $\eta$. See the text for definitions.

Table 6.3. Spearman and Kendall Rank Correlation Tests

| Tested Quantities | | | Spearman | | | Kendall | | | |
|---|---|---|---|---|---|---|---|---|---|
| Absorption (1) | Galaxy (2) | N (3) | $r_{\rm s}$ (4) | $P_{\rm s}$ (5) | $N_\sigma$ (6) | $\tau_{\rm k}$ (7) | $P_{\rm k}$ (8) | $N_\sigma$ (9) | $P_{\rm MC}$ (10) |
| $W_{\rm r}$ | $B-K$ | 13 | −0.54 | 0.07 | 1.83 | −0.43 | 0.04 | 2.03 | 0.04 |
| DR | $D$ | 14 | 0.49 | 0.07 | 1.84 | 0.40 | 0.04 | 2.00 | 0.05 |
| $N_{\rm c}$ | $D$ | 15 | −0.60 | 0.04 | 2.02 | −0.39 | 0.04 | 2.01 | 0.05 |
| $N_A$ | $L_K$ | 14 | −0.58 | 0.04 | 2.10 | −0.43 | 0.03 | 2.14 | 0.06 |
| $A(\Delta v)$ | $D$ | 15 | 0.47 | 0.08 | 1.78 | 0.35 | 0.07 | 1.83 | 0.06 |
| $W_{\rm r}$ | $D$ | 13 | −0.53 | 0.06 | 1.89 | −0.36 | 0.07 | 1.81 | 0.08 |
| DR | $B-K$ | 13 | 0.36 | 0.18 | 1.34 | 0.34 | 0.10 | 1.63 | 0.10 |
| $A(\Delta v)$ | $S$ | 13 | −0.73 | 0.01 | 2.53 | −0.51 | 0.01 | 2.44 | 0.14 |

Note. — Columns 1 and 2 list the absorption and galaxy properties for which the rank correlation tests were performed. Column 3 gives the number of galaxies used in the test. Columns 4 and 7 tabulate $r_{\rm s}$ and $\tau_{\rm k}$, the Spearman correlation coefficient and the Kendall $\tau$, respectively. The probabilities, $P_{\rm s}$ and $P_{\rm k}$, and the number of standard deviations $N_\sigma$ by which the rank coefficients deviate from their null hypothesis values are listed in columns 5, 8, 6, and 9, respectively. In column 10 are the $P_{\rm MC}$ from the Monte–Carlo simulations.

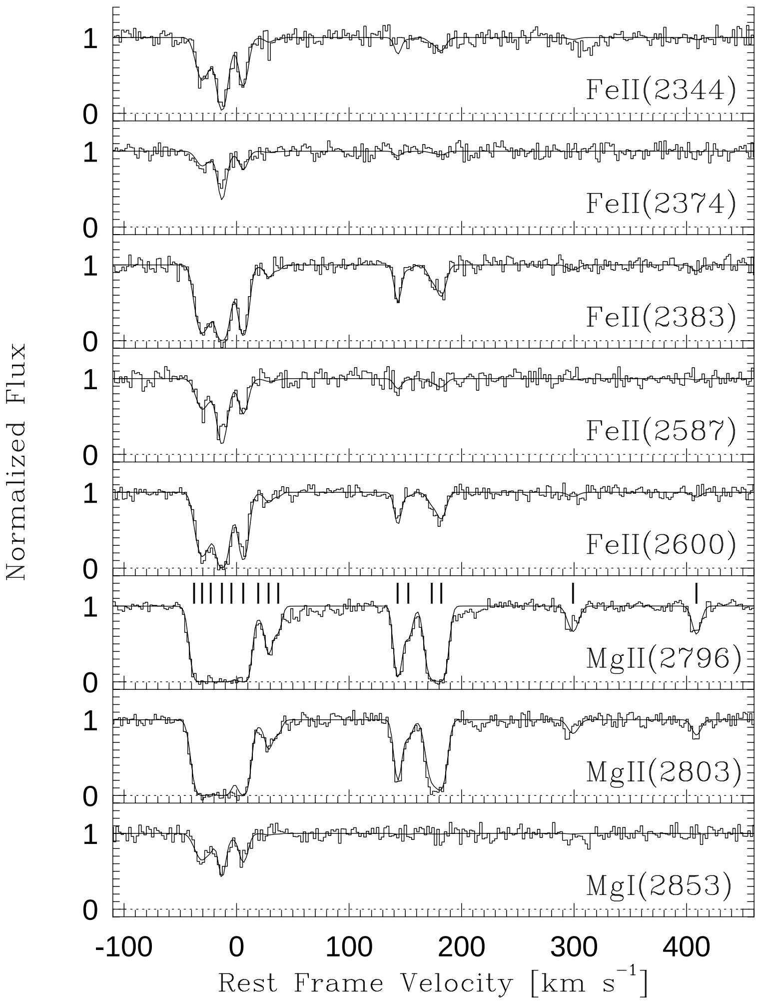


Fig. 6.1.— The multiple transitions observed for G2 with simultaneous profile fits (by hand) shown. The subcomponents from the fit, and their velocities, are shown as vertical ticks above the Mg II $\lambda2796$ transition.

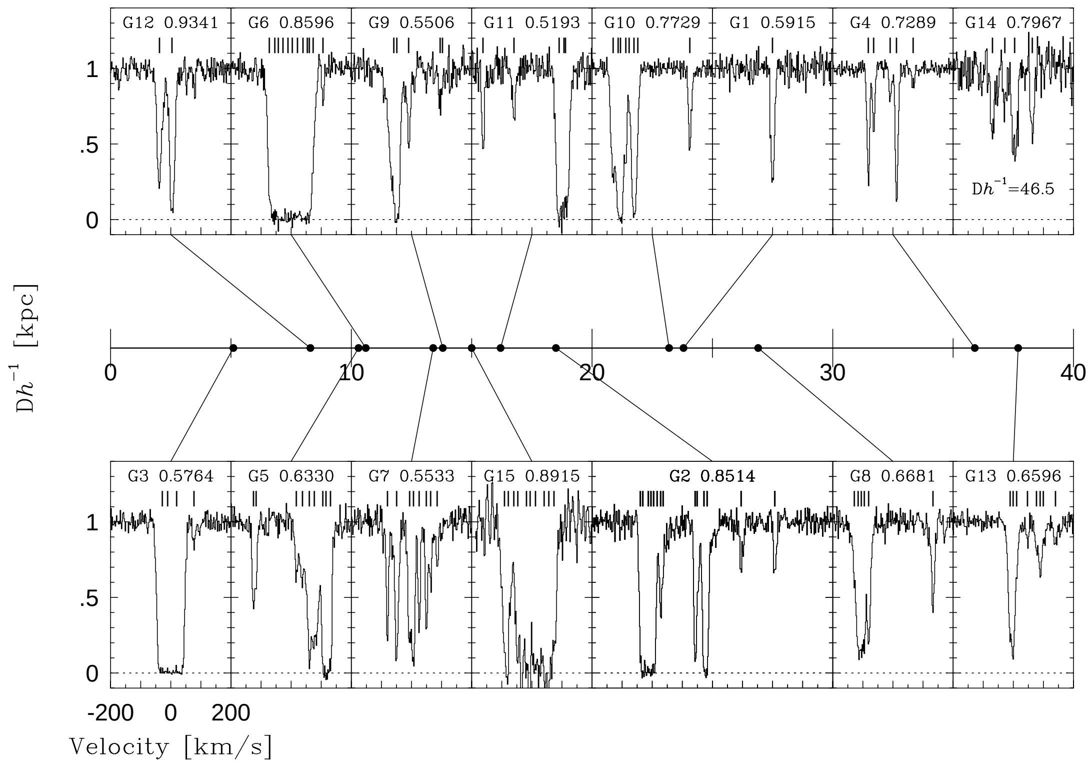


Fig. 6.2.— The Mg II $\lambda2796$ absorption profiles obtained with HIRES on the Keck telescope plotted in order of increasing impact parameter, $Dh^{-1}$ kpc, of the associated absorbing galaxy. The vertical ticks above the continuum of each absorption feature mark the subcomponents used in the analysis.

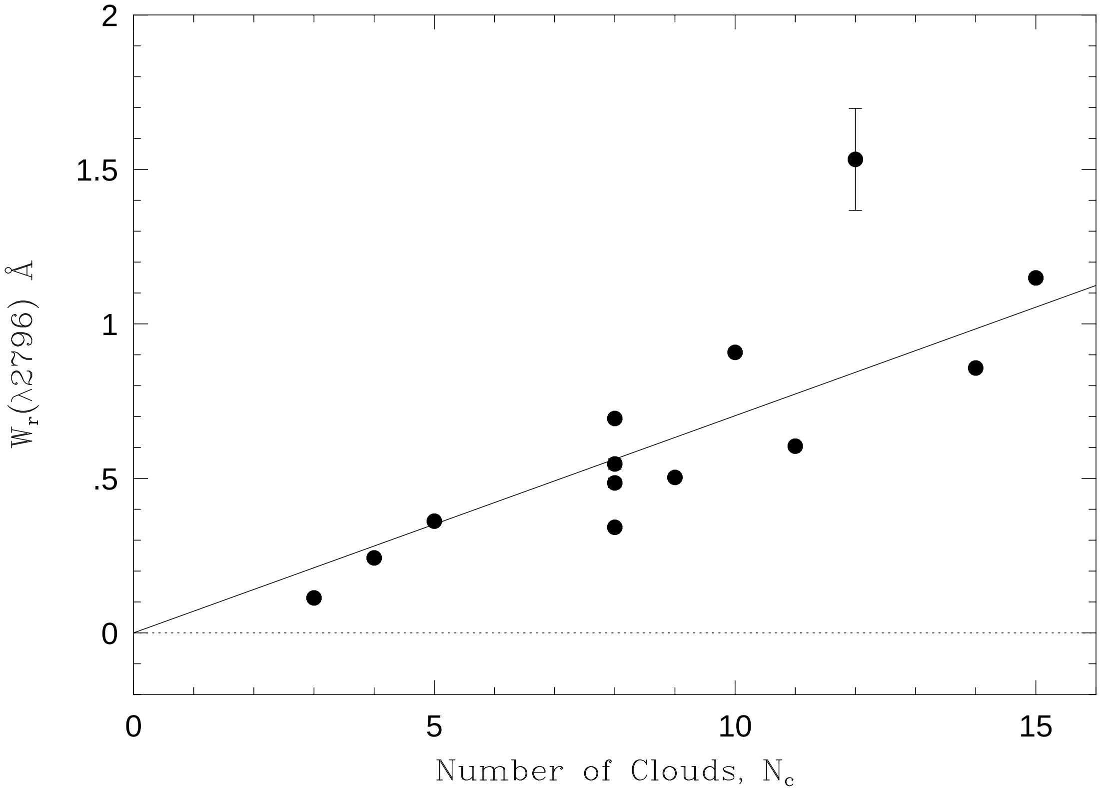


Fig. 6.3.— The rest equivalent width of Mg II $\lambda2796$ versus the number of clouds for 13 of the systems presented in Table 2. The error bars are the formal errors from the spectral analysis and are roughly the size of the data points, with the exception of that measured for G15. The LSF slope has been forced through the origin.

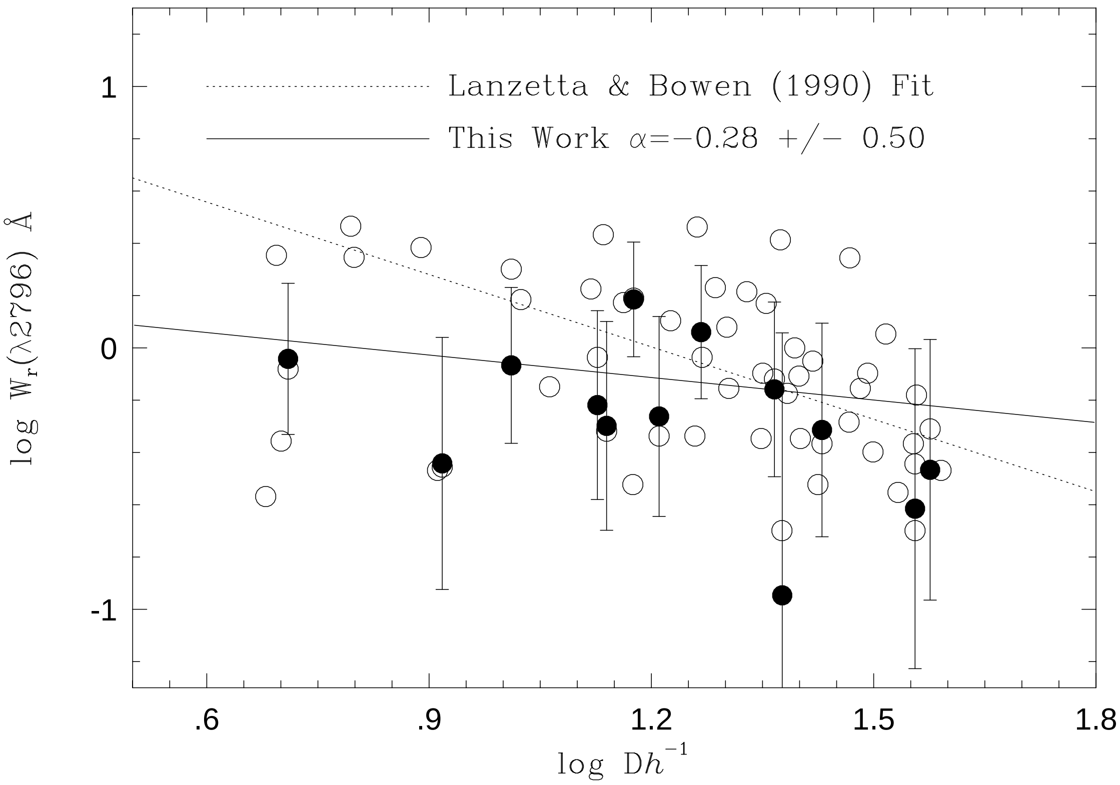


Fig. 6.4.— $W_{\rm r}(\lambda 2796)$ versus the QSO–galaxy impact parameter $D$. The open circles are the $z \leq 1$ SDP dataset and the filled circles are the 13 systems measured in this work. The error bars are the modeled scatter in the $W_{\rm r}$ due to intercepting a finite number of clouds along the line of sight. The dashed line shows the LSF slope to the assumed relationship $W_r = AD^{\alpha}$ found by Lanzetta & Bowen (1990) using a smaller and different data set of Mg II absorbers. The solid line is our LSF result. We found $\alpha = -0.28 \pm 0.50$, which is not a statistically significant slope.

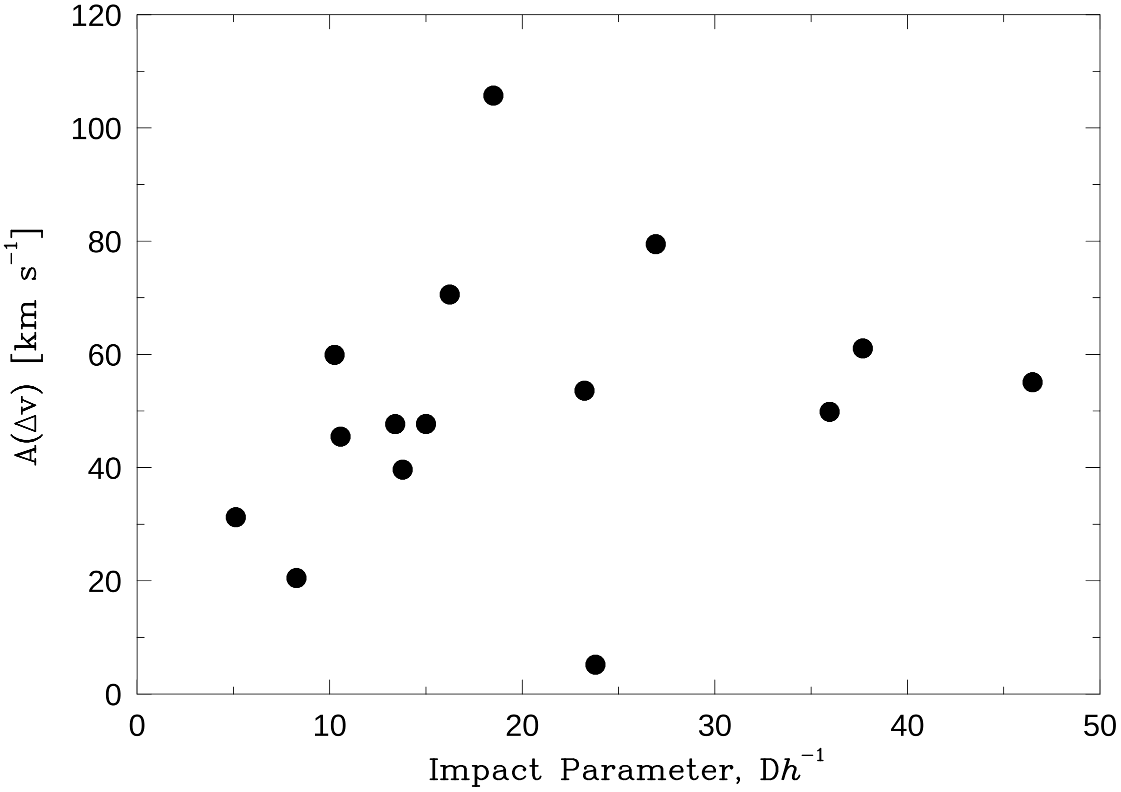


Fig. 6.5.— The median absolute deviation of cloud velocities (equation 1) versus the QSO–galaxy impact parameter. There is no clear trend in the line–of–sight velocity "dispersion" with the projected galactocentric distance probed by the QSO light path. Both the rotational and infall kinematic models of galactic halos predict a decreasing spread with impact parameter (see text).